ORIGINAL ARTICLE

Multiscale Numerical Methods for Modeling Biofluid Dynamics Across Cellular to Organ-Level Scales

Luis Eduardo Martínez[1] and Carlos Andrés Guevara[2]

[1]Universidad del Quindío, Department of Mathematics, Avenida Bolívar, Armenia, Quindío, Colombia.,
[2]Universidad Tecnológica de Pereira, Faculty of Mathematics and Statistics, Carrera 27, Pereira, Risaralda, Colombia.,

ABSTRACT

The multiscale modeling of biofluid dynamics presents a formidable challenge due to the inherent complexity of physiological systems, where interactions span molecular, cellular, tissue, and organ-level scales. This paper systematically examines advanced numerical methodologies tailored to address these cross-scale phenomena, focusing on their mathematical underpinnings, computational trade-offs, and physiological fidelity. We critically evaluate continuum-based approaches, such as the Navier-Stokes equations with hybrid viscoelastic constitutive models, against discrete particle methods, including dissipative particle dynamics and lattice Boltzmann formulations. Special emphasis is placed on interface-capturing techniques like the immersed boundary method and arbitrary Lagrangian-Eulerian frameworks for resolving fluid-structure interactions in deformable biological tissues. Furthermore, we analyze homogenization strategies for bridging cellular-scale phenomena—such as endothelial shear stress sensing—to macroscopic hemodynamic simulations. A comparative assessment of monolithic versus partitioned coupling schemes reveals critical insights into numerical stability and scalability for large-scale vascular simulations. The discussion extends to recent advances in data-driven surrogate modeling, which synergize reduced-order physics with machine learning to alleviate computational bottlenecks. By contextualizing these approaches against experimental validations in vascular flow and pulmonary dynamics, this work provides a rigorous framework for selecting appropriate multiscale strategies based on accuracy, efficiency, and target physiological observables.

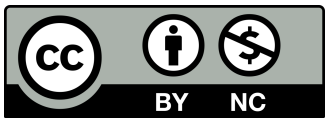

1 | Introduction

Biological fluid dynamics operates across spatial and temporal scales that can differ by multiple orders of magnitude [1]. At the smallest scales, intracellular processes and membrane mechanics unfold on nanometer-length scales and microsecond timescales, while whole-organ phenomena, such as blood circulation in the human cardiovascular system, extend over meters and can evolve over seconds to hours [2]. Traditional single-scale numerical approaches—be they molecular dynamics at the nanometer level or continuum Navier-Stokes models at the organ level—often fail to capture emergent phenomena arising from cross-scale couplings. For instance, the initial stages of thrombus formation, governed by platelet adhesion at the cellular scale, can dramatically alter effective blood viscosity and rheology at the macroscopic level. [3]

To address these challenges, multiscale modeling has emerged as a promising paradigm. In one class of approaches, referred to as hierarchical modeling, fine-scale simulations (e.g., dissipative particle dynamics or molecular dynamics) provide effective parameters, such as viscosity or permeability, to a coarser, continuum-scale model via homogenization [4]. However, this approach can break down when feedback mechanisms from the macro scale significantly impact the micro scale—exemplified by high-shear-rate flows influencing cell membrane conformation [5]. Another class of approaches, termed concurrent or on-the-fly coupling, maintains simultaneous calculations at both micro and macro scales within the same simulation framework. While these methods promise higher fidelity, their computational demands can be prohibitive for large-scale organ-level simulations unless specialized algorithms or high-performance computing resources are employed. [6]

Mathematically, these problems often exhibit mixed hyperbolic-parabolic character and can involve strongly nonlinear constitutive relationships. Stabilized finite elements, finite volumes, or lattice Boltzmann methods are typically employed to handle advection-dominated flows and ensure stability under complex boundary conditions [7]. Additional complications arise when modeling fluid-structure interactions (FSI) in deformable tissues or cells, especially in the presence of active stresses generated by biological processes such as muscle contraction or ciliary beating. These phenomena require specialized numerical coupling schemes, such as the immersed boundary method or arbitrary Lagrangian-Eulerian (ALE) frameworks, that preserve accuracy near moving interfaces. [8]

This work aims to provide a unified treatment of these diverse multiscale modeling methodologies, with a particular focus on the mathematical formulations, discretization strategies, and stabilization methods required for robust simulations of biologically realistic systems [9]. Through illustrative examples in vascular networks, pulmonary airflow, and microvascular endothelial dynamics, we offer guidance on selecting and coupling models at different scales. We further examine the emerging role of machine learning techniques—such as neural-network-based subgrid-scale (SGS) closures or surrogate modeling—to reduce computational overhead while maintaining essential multiscale fidelity. [10]

In what follows, we first establish key mathematical equations and physical models that underpin multiscale biofluid dynamics, from continuum Navier-Stokes systems with viscoelastic stresses down to discrete particle or agent-based frameworks. We then discuss the challenges inherent to modeling cellular and subcellular processes, placing particular emphasis on membrane elasticity and stochastic gating of ion channels [11]. Moving upward in scale, we examine tissue-level and organ-level flow phenomena, including pulmonary dynamics and arterial hemodynamics, and detail how these continuum models couple to fine-scale processes via homogenization or explicit concurrency [12]. Afterward, we compare competing numerical schemes—monolithic versus partitioned coupling, immersed boundary versus ALE, lattice Boltzmann versus finite elements—and highlight the trade-offs between computational cost, numerical stability, and accuracy. We conclude by identifying frontiers in uncertainty quantification, GPU-accelerated computing, and data-driven hybrid methods that promise to shape the next generation of multiscale biofluid simulations. [13]

2 | Foundations of Multiscale Biofluid Dynamics

Mathematical formalisms for multiscale biofluid dynamics must capture macroscopic momentum and mass conservation while accommodating the local rheological complexities often introduced by cellular-scale or molecular-scale behavior. One canonical set of governing equations at the organ or tissue level is the incompressible Navier-Stokes system: [14]

$$\rho\left(\frac{\partial \mathbf{u}}{\partial t} + \mathbf{u}\cdot\nabla\mathbf{u}\right) = -\nabla p + \nabla\cdot\tau + \mathbf{f}_{\text{ext}},$$
$$\nabla\cdot\mathbf{u} = 0,$$

where $\mathbf{u}$ is the velocity field, p is the pressure, ρ is the (generally constant) fluid density, and $\mathbf{f}_{\text{ext}}$ represents external body forces such as gravity or, in some contexts, electromagnetic forces. The term τ is the extra stress tensor, which may be purely Newtonian ($\tau = 2\mu\mathbf{D}$ with $\mathbf{D} = \frac{1}{2}(\nabla\mathbf{u} + (\nabla\mathbf{u})^T)$) or it may encode more complex rheological laws:

$$\tau = \tau(\mathbf{u}, \dot\gamma, \cdots),$$

where $\dot\gamma$ denotes the magnitude of the shear rate. In viscoelastic or shear-thinning models such as Carreau-Yasuda or Cross, the effective viscosity $\mu(\dot\gamma)$ can decrease significantly with increasing shear rate:

$$\mu(\dot\gamma) = \mu_\infty + (\mu_0 - \mu_\infty)\left[1 + (\lambda\dot\gamma)^2\right]^{\frac{n-1}{2}}.$$

Hybrid Continuum-Viscoelastic Formulations. In many biological flows—particularly in blood, mucus, or other polymeric fluids—viscoelastic behavior is essential. One widely used approach is to augment the Navier-Stokes system with an evolution equation for the polymeric stress τ_p. For example, the Oldroyd-B model can be written as: [15]

$$\frac{\partial \tau_p}{\partial t} + \mathbf{u}\cdot\nabla\tau_p = \tau_p\cdot(\nabla\mathbf{u}) + (\nabla\mathbf{u})^T\cdot\tau_p - \frac{1}{\lambda_1}(\tau_p - \eta_p\mathbf{D}),$$
$$\tau = \tau_s + \tau_p,$$

where λ_1 is a relaxation time, η_p is the polymer viscosity, and $\tau_s = 2\eta_s\mathbf{D}$ is the solvent (Newtonian) contribution. Similar forms exist for the Giesekus, FENE-P, or Phan-Thien–Tanner (PTT) models, each capturing different rheological phenomena such as shear-thinning or strain-hardening. [16]
The Giesekus model introduces an additional nonlinear stress term to account for anisotropic drag effects in polymer solutions:

$$\frac{\partial \tau_p}{\partial t} + \mathbf{u}\cdot\nabla\tau_p = \tau_p\cdot(\nabla\mathbf{u}) + (\nabla\mathbf{u})^T\cdot\tau_p - \frac{1}{\lambda_1}(\tau_p - \eta_p\mathbf{D} + \alpha\tau_p^2),$$

where α is a mobility parameter that influences shear-thinning behavior [17]. In contrast, the FENE-P model modifies the polymer stress evolution by incorporating a finite extensibility parameter L that bounds polymer elongation:

$$\frac{\partial \tau_p}{\partial t} + \mathbf{u}\cdot\nabla\tau_p = \tau_p\cdot(\nabla\mathbf{u}) + (\nabla\mathbf{u})^T\cdot\tau_p - \frac{1}{\lambda_1}\left(\frac{\tau_p - \eta_p\mathbf{D}}{1 - \frac{\mathrm{tr}(\tau_p)}{L^2}}\right).$$

This formulation is particularly effective for modeling DNA-laden biofluids or polymer networks in mucus transport [18]. The Phan-Thien–Tanner (PTT) model further extends this framework by incorporating strain-dependent relaxation effects: [19]

$$\frac{\partial \tau_p}{\partial t} + \mathbf{u}\cdot\nabla\tau_p = \tau_p\cdot(\nabla\mathbf{u}) + (\nabla\mathbf{u})^T\cdot\tau_p -$$
$$\frac{1}{\lambda_1}\left(\tau_p - \eta_p\mathbf{D} + \frac{\epsilon}{\lambda_1}\mathrm{tr}(\tau_p)\tau_p\right),$$

where ϵ modulates the strain-hardening response. Each of these constitutive models introduces additional computational challenges, necessitating specialized numerical schemes such as logarithmic conformation tensor methods or spectral element discretizations to maintain stability in high-Weissenberg-number regimes [20, 21]. Hybrid formulations that couple viscoelastic models with generalized Newtonian viscosity corrections have also been proposed to enhance accuracy in simulations of blood flow, where both viscoelasticity and shear-thinning must be simultaneously accounted for.

Discrete Particle Representations. At micro- or nano-scales, continuum approaches may no longer suffice, especially if individual red blood cells, platelets, or macromolecules must be resolved [22]. Particle-based methods such as dissipative particle dynamics (DPD) or smoothed particle hydrodynamics (SPH) discretize the fluid into mesoscale particles that interact via forces designed to reproduce Navier-Stokes-like behavior at larger scales. For instance, in DPD: [23]

$$m_i\frac{d\mathbf{v}_i}{dt} = \sum_{j\neq i}\left(\mathbf{F}_{ij}^C + \mathbf{F}_{ij}^D + \mathbf{F}_{ij}^R\right),$$

where $\mathbf{F}_{ij}^C$ is a conservative force that can model local repulsions or attractions, $\mathbf{F}_{ij}^D$ is a dissipative force proportional to velocity differences (reflecting viscous effects), and $\mathbf{F}_{ij}^R$ is a random force that simulates thermal fluctuations. By tuning these parameters, one can match desired viscosity and compressibility properties. [24]
SPH, in contrast, represents the fluid as a set of discrete particles carrying mass, momentum, and sometimes energy, with interpolation kernels

$W(\mathbf{x}-\mathbf{x}_j, h)$ defining local averaging over a smoothing length h. The SPH approximation for the continuity equation is given by:

$$\frac{d\rho_i}{dt} = \sum_j m_j \mathbf{v}_{ij} \cdot \nabla W_{ij},$$

where ρ_i is the density at a given particle position, m_j is the mass of neighboring particles, and $\mathbf{v}_{ij} = \mathbf{v}_i - \mathbf{v}_j$ represents velocity differences. The corresponding momentum equation takes the form: [25]

$$\frac{d\mathbf{v}_i}{dt} = -\sum_j m_j \left(\frac{p_i}{\rho_i^2} + \frac{p_j}{\rho_j^2} + \Pi_{ij} \right) \nabla W_{ij},$$

where p_i and p_j are pressure values assigned to particles and Π_{ij} represents artificial viscosity terms required for numerical stability in high-shear flows. The coupling of discrete particle data to continuum fields often hinges on coarse-graining operators, $\mathcal{C}[\cdot]$, that map particle-scale forces or stress distributions onto continuum variables:

$$\tau(\mathbf{x}, t) = \mathcal{C}\left[\{\mathbf{F}_{ij}\}, \{\mathbf{x}_i\}, \{\mathbf{v}_i\}\right].$$

In turn, the continuum velocity $\mathbf{u}(\mathbf{x}, t)$ can feed back into particle boundary conditions or flow fields, enabling two-way coupling in concurrent simulations. Hybrid models, where a Navier-Stokes solver governs macroscopic flow while a DPD or SPH subdomain resolves microscale interactions, have been employed to simulate red blood cell aggregation, platelet adhesion, and transport of drug-laden nanoparticles in blood plasma. These multiscale approaches allow direct incorporation of cellular-scale mechanics into whole-organ hemodynamic simulations, capturing non-Newtonian effects emerging from discrete particle interactions. [26]

Stabilized Discretizations and Ill-Posedness. Nonlinear coupling between micro- and macro-scales, along with viscoelastic or shear-thinning laws, can introduce ill-posedness or severe stiffness in the governing PDEs [27]. For instance, combining strongly convective flows (large Reynolds numbers) with nearly elastic fluid behavior (high Deborah or Weissenberg numbers) may lead to numerical instabilities, requiring advanced stabilization. Residual-based stabilizations such as SUPG (streamline-upwind Petrov-Galerkin) add selective artificial diffusion along characteristic directions: [28]

$$\int_\Omega \rho(\mathbf{u}\cdot\nabla\mathbf{u})\cdot\mathbf{v}_h \, d\Omega \;\to\; \int_\Omega \rho(\mathbf{u}\cdot\nabla\mathbf{u})\cdot\mathbf{v}_h \, d\Omega$$
$$+ \sum_K \int_K \tau_{\text{SUPG}} (\rho\,\mathbf{u}\cdot\nabla\mathbf{R}_u)(\mathbf{u}\cdot\nabla\mathbf{v}_h),$$

where $\mathbf{R}_u$ is the momentum residual and τ_{SUPG} is a stabilization parameter that depends on element size, velocity magnitude, and time step. Without such stabilizations, high-order methods or standard Galerkin discretizations can develop oscillatory solutions or fail to converge. [29]

In sum, constructing robust and accurate mathematical foundations for multiscale biofluid dynamics requires reconciling continuum PDEs for momentum and mass conservation, discrete particle formulations at smaller scales, and possibly additional PDEs for viscoelastic or polymeric stresses. The subsequent sections explore how these mathematical foundations integrate with specific biological processes and simulation frameworks at smaller (cellular) and larger (tissue or organ) scales. [30]

3 | Cellular and Subcellular Scale Modeling

Biological cells embedded in a fluid environment experience a wide array of forces, from external shear stresses due to flow, to intracellular tension governed by cytoskeletal dynamics and membrane elasticity [31]. Accurate modeling at these scales often necessitates discrete or hybrid methods that can capture membrane deformations, stochastic biochemical reactions, and complex interactions between cells.

Membrane Elasticity and Particle-Based Descriptions. One popular approach for red blood cell (RBC) or platelet-scale modeling involves a network of springs (or triangulated surfaces) representing the cell membrane: [32]

$$U_{\text{membrane}} = \sum_{\langle i,j \rangle} \frac{k_s}{2} \big(||\mathbf{x}_i - \mathbf{x}_j|| - l_0\big)^2 + \sum_{\langle \alpha,\beta \rangle} k_b(\theta_{\alpha,\beta} - \theta_0)^2,$$

where the first sum is over edges $\langle i, j \rangle$ connecting membrane vertices $\mathbf{x}_i$ and $\mathbf{x}_j$, each with a rest length l_0, and the second sum penalizes deviations in local bending angles $\theta_{\alpha,\beta}$. The associated forces, $\mathbf{F}_{ij} = -\nabla_{\mathbf{x}_i} U_{\text{membrane}}$, couple into either a dissipative particle dynamics (DPD) framework or a continuum fluid solver via immersed boundary methods.

In this representation, the membrane's in-plane elasticity emerges from the stretching term, ensuring that local deformations remain within physiological constraints. The bending energy term, in contrast, governs the out-of-plane flexibility of the membrane,

which is crucial for capturing the deformability of RBCs under shear flow [33]. The parameters k_s and k_b are typically tuned to match experimental measurements of cell deformation indices and membrane fluctuation spectra. [34]
A more sophisticated membrane model includes area and volume conservation constraints, necessary for modeling nearly-incompressible lipid bilayers:

$$U_{\text{area}} = \frac{k_A}{2}(A - A_0)^2, \quad U_{\text{volume}} = \frac{k_V}{2}(V - V_0)^2,$$

where A and V are the instantaneous surface area and volume, respectively, and A_0, V_0 are their reference values [35, 36]. The parameters k_A and k_V enforce global conservation properties, ensuring that the membrane does not undergo unrealistic shrinkage or expansion due to numerical artifacts.
To integrate these forces into a fluid solver, a particle-based approach such as DPD is commonly employed [37]. In DPD, the membrane vertices interact with surrounding fluid particles via hydrodynamic forces, allowing for a direct coupling between the cellular structure and the surrounding medium. This interaction is typically mediated through a Langevin-like formalism, incorporating both deterministic and stochastic forces: [38]

$$m_i \frac{d\mathbf{v}_i}{dt} = \sum_{j \neq i} (\mathbf{F}_{ij}^C + \mathbf{F}_{ij}^D + \mathbf{F}_{ij}^R) + \mathbf{F}_i^{\text{membrane}},$$

where $\mathbf{F}_i^{\text{membrane}}$ represents the elastic and bending forces exerted by the membrane model.
Another widely used approach is to embed the membrane model within a smoothed particle hydrodynamics (SPH) framework, where the fluid dynamics are solved using a Lagrangian description [39]. In this case, the membrane particles carry additional information, such as curvature and tension, which influences their interaction with surrounding fluid particles. By carefully tuning the interaction kernels, SPH-based models can achieve accurate representations of RBC and platelet deformation under physiological shear conditions. [40]

Immersed Boundary Methods for Cell Deformations. The immersed boundary (IB) method provides a particularly elegant technique for coupling elastic structures, like cell membranes or filament networks, to an incompressible fluid. In this framework, the membrane is represented by a set of Lagrangian markers $\mathbf{X}(s,t)$, where s parameterizes the membrane surface. These markers exert forces onto the surrounding fluid, which in turn influences their motion [41]. The governing equations for the IB method are: [42]

$$\rho \left(\frac{\partial \mathbf{u}}{\partial t} + \mathbf{u} \cdot \nabla \mathbf{u} \right) = -\nabla p + \mu \nabla^2 \mathbf{u} + \int_\Gamma \mathbf{F}(s,t)\, \delta(\mathbf{x} - \mathbf{X}(s,t))\, ds.$$

Here, the force $\mathbf{F}(s,t)$ is derived from the membrane elasticity model and is distributed to the Eulerian grid via a discrete Dirac delta function $\delta(\mathbf{x} - \mathbf{X}(s,t))$. The motion of the membrane markers is then updated by interpolating the fluid velocity:

$$\frac{\partial \mathbf{X}}{\partial t}(s,t) = \int_\Omega \mathbf{u}(\mathbf{x},t)\, \delta(\mathbf{x} - \mathbf{X}(s,t))\, d\mathbf{x}.$$

A key advantage of the IB method is that it allows for complex boundary deformations without the need for explicit mesh generation around moving structures [43]. This is particularly important in simulations of RBCs and platelets, which undergo extreme shape changes as they traverse microvascular networks. The IB method also naturally accommodates the effects of fluid-structure interactions, including the formation of membrane tethers and vesicle rupture under high shear conditions. [44]
To ensure numerical stability in large deformation regimes, specialized discretization techniques are employed for the delta function. One common approach is to use a regularized delta function, such as: [45, 46]

$$\delta_h(\mathbf{x}) = \frac{1}{h^3} \phi\left(\frac{x}{h}\right) \phi\left(\frac{y}{h}\right) \phi\left(\frac{z}{h}\right),$$

where $\phi(r)$ is a smooth function that preserves interpolation accuracy while preventing numerical oscillations. [47]
The IB method can also be extended to incorporate active cellular processes, such as cytoskeletal remodeling and adhesion dynamics. For example, actin polymerization forces at the leading edge of migrating cells can be modeled by introducing additional source terms in the force equation: [48]

$$\mathbf{F}_{\text{actin}} = k_{\text{polymer}}(\mathbf{X} - \mathbf{X}_0),$$

where k_{polymer} represents the polymerization rate and $\mathbf{X}_0$ is the reference position of the membrane. Such formulations allow for the simulation of platelet aggregation, leukocyte rolling, and endothelial cell deformation in response to mechanical stimuli.
In hybrid computational models, IB techniques are often coupled with continuum-based solvers for non-Newtonian blood flow [49]. A typical example is the combination of an IB membrane model with a

finite element fluid solver using a Carreau-Yasuda viscosity model: [50]

$$\eta(\dot{\gamma}) = \eta_\infty + (\eta_0 - \eta_\infty)\left[1 + (\lambda\dot{\gamma})^a\right]^{\frac{n-1}{a}}.$$

This coupling allows for the accurate simulation of shear-thinning effects in plasma while resolving individual RBC dynamics. Further refinements include multiscale coupling strategies, where molecular-scale interactions (such as membrane protein dynamics) are incorporated via coarse-graining techniques [51]. Such approaches have been employed to model malaria-infected RBCs, whose altered mechanical properties significantly impact microcirculatory flow. The combination of membrane elasticity models, particle-based descriptions, and immersed boundary formulations provides a powerful framework for studying cell-scale hemodynamics [52]. By integrating these techniques into hybrid numerical solvers, researchers can achieve unprecedented resolution in simulating the complex interplay between cellular mechanics and blood flow. These advancements have direct applications in understanding pathological conditions such as sickle cell disease, clot formation, and targeted drug delivery in microvascular networks. [53]

Biochemical Transport and Reaction Kinetics. Cells also sense and respond to their chemical environment, leading to advection-diffusion-reaction equations for signaling molecules such as adenosine diphosphate (ADP) in platelet aggregation or Ca^{2+} in muscle contraction. A typical PDE system might be: [54]

$$\frac{\partial c}{\partial t} + \nabla \cdot (c\,\mathbf{u}) = D\nabla^2 c + R(c),$$
$$c(\mathbf{x}, 0) = c_0(\mathbf{x}),$$

where c is the concentration of the signaling molecule, D is the diffusion coefficient, and $R(c)$ represents local reaction kinetics (e.g., enzymatic production or decay terms). At the cell boundary, boundary conditions can encode fluxes dependent on receptor-ligand binding or mechanochemical coupling. [55]

Stochastic Ion Channel Dynamics. Cellular excitability, seen in cardiomyocytes or neurons, arises from the stochastic gating of ion channels, frequently modeled by a Hodgkin-Huxley framework with noise:

$$C_m \frac{dV}{dt} = I_{\text{ext}} - \sum_i g_i m_i^p h_i^q (V - E_i) + \xi(t),$$

where V is the transmembrane potential, g_i is the maximum conductance for ion channel type i, E_i is the reversal potential, and $\xi(t)$ is a stochastic term capturing random channel openings/closings [56]. Coupling these cellular electrophysiology models to fluid flow can be crucial for phenomena like mechanotransduction in endothelial cells, where shear stress modulates ion channel kinetics and thus affects intracellular signaling pathways. [57]
The integration of these subcellular details into larger-scale fluid simulations is challenging. One must define appropriate coupling interfaces, ensuring that mechanical stresses in the fluid update the cell membrane state, while in turn, cell deformations or secreted chemicals feed back into the local flow field [58]. This concurrency may be updated at each time step or in a loosely coupled manner if the timescales of cell responses are much slower than the fluid dynamics.

4 | Tissue and Organ-Level Fluid Dynamics

Moving from cellular microenvironments to tissues and entire organs involves yet another leap in characteristic length and time scales [59]. Two essential areas illustrating this complexity are pulmonary airflow in the lung and blood flow in large vascular networks, such as coronary or cerebral arteries.

Pulmonary Airflow and Tissue Mechanics. Breathing involves not only airflow within the branching bronchial tree but also expansion and contraction of alveolar sacs, whose walls exhibit complex viscoelastic and surface tension behaviors [60]. A continuum approach for the lung parenchyma may involve modeling alveolar tissue as a viscoelastic material with a stress-strain relationship: [61, 62]

$$\mathbf{S}(\mathbf{E}, t) = \frac{\partial W}{\partial \mathbf{E}} + \int_0^t G(t-\tau)\,\frac{\partial \mathbf{E}}{\partial \tau}\,d\tau,$$

where W is a hyperelastic strain-energy function, and G captures stress relaxation effects. The viscoelastic properties of lung parenchyma arise due to its composition of extracellular matrix proteins, including elastin and collagen, which contribute to both its elastic recoil and time-dependent stress relaxation [63]. Alveolar walls are lined with a thin layer of pulmonary surfactant, reducing surface tension and preventing alveolar collapse, a phenomenon known as atelectasis. The dynamics of surfactant distribution across the alveolar interface can be described using transport

equations coupled with the fluid dynamics of the airway. [64]
Coupling alveolar tissue deformation to the fluid equations in the bronchial tree can be achieved via an Arbitrary Lagrangian-Eulerian (ALE) scheme: [65]

$$\frac{\partial \mathbf{u}}{\partial t}\Big|_{\mathbf{X}(\mathbf{x},t)} + \left[(\mathbf{u}-\mathbf{w})\cdot\nabla\right]\mathbf{u} = -\frac{1}{\rho}\nabla p + \nu\nabla^2\mathbf{u},$$

where $\mathbf{w}$ is the local mesh velocity of the moving alveolar boundary and $\mathbf{X}(\mathbf{x},t)$ describes the mapping from reference to current configuration. The ALE framework allows for the tracking of the alveolar boundary motion, which is essential in resolving the interaction between airflow and lung parenchymal deformation.
A comprehensive computational model of pulmonary mechanics should account for the multi-scale nature of the lung, spanning from the macroscopic airway tree to the microscopic alveolar structures [66]. The airway resistance to airflow can be estimated using the Poiseuille law for laminar flow in small bronchioles:

$$R = \frac{8\mu L}{\pi r^4},$$

where R is the airway resistance, μ is the dynamic viscosity of air, L is the airway length, and r is the airway radius [67]. However, turbulence and secondary flows in larger airways require a more complex treatment, such as direct numerical simulation (DNS) or large-eddy simulation (LES).
Incorporating regional heterogeneity in lung mechanics is crucial for accurate simulation of pulmonary airflow and tissue deformation [68]. Factors such as gravity-dependent variations in alveolar expansion, localized airway obstructions, and non-uniform surfactant distribution introduce spatial complexity into the lung's mechanical behavior [69].
High-resolution imaging modalities, such as four-dimensional computed tomography (4D-CT) and hyperpolarized MRI, provide essential data for validating computational models.

Coronary and Large-Vessel Hemodynamics. Arterial blood flow in large vessels can be approximated by the Navier-Stokes equations with shear-thinning viscosity if necessary [70]. However, when coupling to myocardial tissue for modeling perfusion, one must solve the poroelastic Biot equations:

$$\begin{aligned} \nabla\cdot\left(\sigma_{\text{solid}} - \alpha p\,\mathbf{I}\right) &= 0, \\ \frac{\partial\phi}{\partial t} + \nabla\cdot\mathbf{q} &= 0, \end{aligned} \qquad \mathbf{q} = -\frac{\kappa}{\mu}\Big(\nabla p - \rho_f \mathbf{g}\Big),$$

where ϕ is the fluid porosity, κ is the permeability, and p is the fluid pressure [71]. The stress σ_{solid} in the solid matrix couples to the fluid pressure p, and α is a Biot–Willis parameter that accounts for fluid-solid interaction.
In large arteries, the Windkessel effect plays a crucial role in maintaining continuous blood flow despite the pulsatile nature of cardiac output [72]. The compliance of arterial walls enables energy storage during systole and release during diastole, mitigating fluctuations in blood pressure. The pressure-flow relationship in large arteries can be approximated using a lumped-parameter Windkessel model: [73]

$$P(t) = P_0 + \frac{Q(t)R}{1 + RCd/dt},$$

where $P(t)$ is the arterial pressure, $Q(t)$ is the volumetric flow rate, R is the vascular resistance, and C is the arterial compliance.
Coronary circulation presents additional complexities due to the interaction between blood flow and myocardial contraction [74]. During systole, the intramyocardial pressure compresses coronary vessels, impeding perfusion, whereas diastole is the primary phase for coronary filling. This phenomenon necessitates the use of time-dependent boundary conditions in computational models of coronary hemodynamics. [75, 76]
Myocardial microcirculation, governed by capillary and venular flow, plays a vital role in oxygen delivery and metabolic regulation [77]. The Krogh cylinder model provides a simplified framework for understanding oxygen diffusion from capillaries to surrounding myocardial tissue. However, more sophisticated computational approaches, such as multi-compartment reaction-diffusion models, are often required to capture the complex interaction between flow, metabolism, and autoregulatory mechanisms. [78]
Accurate modeling of coronary hemodynamics has important clinical implications, particularly in the assessment of ischemic heart disease and the optimization of revascularization strategies such as coronary artery bypass grafting (CABG) and percutaneous coronary intervention (PCI).
Hemodynamic simulations can aid in predicting the functional significance of arterial stenoses and optimizing treatment strategies for improved patient outcomes. [79]

Multidimensional Reduced-Order Modeling. In many practical applications, a full 3D simulation of an entire vascular network is prohibitively expensive [80]. Instead, 1D or 2D reduced-order models may be

Parameter	Typical Value	Description
Lung compliance (C_L)	0.2 L/cmH_2O	Measure of lung elasticity, defined as the change in volume per unit pressure change.
Airway resistance (R_A)	1.5 cmH_2O/L/s	Resistance to airflow, influenced by airway diameter and air viscosity.
Alveolar surface tension (γ)	30 mN/m (before surfactant)	Determines the collapsing pressure of alveoli, modified by surfactant to prevent atelectasis.

Table 1: Key physiological parameters influencing pulmonary airflow and alveolar mechanics.

Parameter	Typical Value	Description
Cardiac output (Q)	5 L/min	Total volume of blood pumped by the heart per minute.
Coronary blood flow (Q_c)	250 mL/min	Blood flow through the coronary circulation, supplying oxygen to the myocardium.
Arterial compliance (C)	1.5 mL/mmHg	Ability of arteries to expand and contract in response to pressure changes.

Table 2: Key hemodynamic parameters relevant to large-vessel and coronary circulation.

used, especially for large-scale systemic circulation. A common approach for 1D arterial pulse wave propagation is: [81]

$$\frac{\partial A}{\partial t} + \frac{\partial Q}{\partial x} = 0,$$
$$\frac{\partial Q}{\partial t} + \frac{\partial}{\partial x}\Big(\frac{Q^2}{A}\Big) + \frac{A}{\rho}\frac{\partial p}{\partial x} = -f_r\frac{Q}{A},$$

where $A(x,t)$ is the cross-sectional area of the vessel, $Q(x,t)$ is the volumetric flow rate, and the friction term f_r typically depends on viscosity. A constitutive relationship relates p and A, e.g., [82]

$$p = p_{\text{ext}} + \beta\big(\sqrt{A} - \sqrt{A_0}\big),$$

where β encapsulates arterial stiffness. Such reduced-order models can be coupled at inlets or outlets of 3D simulations, effectively forming a multiscale approach that saves computational cost while preserving essential wave reflection dynamics. [83]

Adaptive Mesh Refinement in Large Domains. An additional strategy in large-organ simulations is adaptive mesh refinement (AMR) or *hp*-adaptivity [84]. Regions near stenoses or branch points may feature steep velocity gradients and require local mesh refinement or higher polynomial order. Meanwhile, uniform refinement of the entire vascular domain is avoided to reduce the overall computational burden [85]. In parallel computing environments, dynamic load balancing must be employed so that refined regions do not cause severe load imbalances across processor ranks.

Overall, bridging from the cellular scale to organ-level mechanics necessitates careful attention to how boundary conditions, constitutive laws, and model assumptions scale up [86]. The next section will delve into the numerical strategies that couple such disparate scales, comparing monolithic approaches with partitioned or hybrid methods and highlighting the trade-offs in stability, complexity, and computational cost. [87, 88]

5 | Comparative Analysis of Multiscale Methodologies

Numerical coupling strategies for multiscale biofluid problems can be broadly grouped into monolithic (fully coupled) and partitioned (segregated) methods. Each offers distinct advantages and challenges in terms of numerical stability, scalability, and ease of

implementation. [89]

Monolithic Coupling and Strongly Coupled Systems. In monolithic approaches, one assembles a global system of equations for all unknowns—fluid velocities, pressures, structural displacements, polymeric stresses, etc.—and solves them simultaneously. This can be conceptualized as: [90]

$$\begin{bmatrix} \mathbf{A} & \mathbf{B}^T \\ \mathbf{B} & \mathbf{C} \end{bmatrix} \begin{bmatrix} \Delta \mathbf{u} \\ \Delta \mathbf{d} \end{bmatrix} = - \begin{bmatrix} \mathbf{R}_u \\ \mathbf{R}_d \end{bmatrix},$$

where $\mathbf{u}$ might represent fluid variables (including velocities and pressures in a mixed formulation) and $\mathbf{d}$ represents structural or additional state variables (e.g., conformation tensor, displacement in the alveolar walls, RBC membrane deformation). The blocks $\mathbf{A}$, $\mathbf{B}$, $\mathbf{C}$ stem from partial derivatives of the residual function $\mathbf{R}_u, \mathbf{R}_d$. A Newton-Raphson approach can be used to handle nonlinearities. While monolithic coupling ensures that fluid-structure or fluid-polymer interactions are resolved consistently at each iteration, the Jacobian system can become extremely large and ill-conditioned, requiring sophisticated linear solvers and preconditioners (e.g., block factorization or approximate Schur complements). [91]

Partitioned and Segregated Schemes. In a partitioned scheme, one solves fluid and structural problems separately, exchanging boundary conditions at each sub-iteration or time step: [92]

$$\mathbf{u}^{(k+1)} = \mathcal{F}\Big(\mathbf{d}^{(k)}\Big), \quad \mathbf{d}^{(k+1)} = \mathcal{S}\Big(\mathbf{u}^{(k+1)}\Big),$$

where $\mathcal{F}$ and $\mathcal{S}$ denote the fluid and structural solvers, respectively. This approach can leverage existing single-physics codes, but it risks instabilities such as the added-mass effect in incompressible fluid-structure systems, where the inertia of the fluid can destabilize the structural update unless relaxation or sub-iterations are introduced:

$$\mathbf{d}^{(k+1)} \leftarrow \mathbf{d}^{(k)} + \omega\big(\mathbf{d}^{(k+1)} - \mathbf{d}^{(k)}\big).$$

Choosing an optimal relaxation parameter ω is crucial to ensure convergence and avoid oscillatory coupling or divergence in strongly coupled regimes (e.g., flexible valves in high-speed flow) [93]. Despite these potential pitfalls, partitioned schemes are often more computationally tractable for large-scale problems because each subproblem can be solved by specialized solvers optimized for fluid or structural equations.

Lattice Boltzmann Methods (LBM) in Biofluid Applications. LBM has gained popularity for simulating complex geometries and multi-phase flows, thanks to its explicit stream-and-collide algorithm and natural parallelization: [94]

$$f_i(\mathbf{x} + \mathbf{e}_i \Delta t, t + \Delta t) - f_i(\mathbf{x}, t) = -\frac{1}{\tau}\big(f_i - f_i^{\mathrm{eq}}\big),$$

where f_i represents particle distribution functions in discrete velocity directions $\mathbf{e}_i$. Macroscopic fields such as $\rho, \mathbf{u}$ are recovered through velocity-moment summations of f_i. Extensions of LBM to non-Newtonian fluids often modify the collision operator or local relaxation time τ to reflect local shear-thinning [95]. Immersing complex moving boundaries (e.g., valves or RBCs) can be handled with bounce-back or interpolated boundary schemes, though the fidelity near highly deformable interfaces remains an active research area.

Hybrid Continuum-Particle Approaches. Concurrent multiscale modeling sometimes combines a continuum solver (finite elements or LBM) for the bulk flow with a particle-based solver (DPD or molecular dynamics) in regions requiring fine-scale resolution: [96]

$$\mathbf{u}_{\mathrm{macro}}(\mathbf{x}, t) = \mathcal{H}\Big(\{\mathbf{v}_i\}\Big),$$
$$\{\mathbf{v}_i\} = \mathcal{G}\Big(\mathbf{u}_{\mathrm{macro}}(\mathbf{x}, t)\Big),$$

where $\mathcal{H}$ and $\mathcal{G}$ are upscaling and downscaling operators that map particle velocities $\{\mathbf{v}_i\}$ to continuum fields $\mathbf{u}_{\mathrm{macro}}$ and vice versa. Momentum conservation is enforced by exchanging forces at an overlapping region or interface. While promising, these methods introduce complexities in interface consistency, parallel load balancing, and the design of smooth bridging zones that avoid spurious reflections of molecular waves at the continuum boundary. [97]

Machine-Learned Surrogate Models. To reduce computational overhead, especially when bridging large scale differences, data-driven surrogates or reduced-order models (ROMs) can approximate the fine-scale physics. For example, one might train a neural network $\mathcal{N}_\theta$ to emulate the subgrid-scale stress:

$$\tau_{\mathrm{SGS}} \approx \mathcal{N}_\theta\big(\mathbf{u}, \nabla \mathbf{u}, \mathrm{Re}, \dots\big),$$

which can then be inserted into a coarse mesh simulation [98]. A distinct advantage is that the surrogate can be trained offline using high-fidelity

data, potentially from experimental measurements (e.g., particle image velocimetry) or from expensive microscale simulations [99]. However, ensuring generalization beyond the training set remains a challenge, especially when the flow regime changes significantly.

In summary, no single method unequivocally outperforms all others in multiscale biofluid applications [100]. Rather, the choice depends on the physics of interest (e.g., degree of compressibility, viscoelastic timescales, presence of large deformations), the geometry (e.g., complex vascular networks vs. simpler chamber flows), and available computational resources [101]. Monolithic approaches can offer robust coupling but may become intractable at scale; partitioned methods are more modular but require careful stabilization and iteration; and hybrid continuum-particle schemes can capture microscopic detail but risk large overhead [102, 103]. Data-driven surrogates further enrich the landscape by alleviating some of the computational burdens, albeit at the expense of requiring extensive training datasets.

6 | Conclusion

Multiscale biofluid modeling stands at the confluence of applied mathematics, computational physics, and biological sciences, offering a powerful framework for understanding the complex, hierarchical organization of physiological flows [104]. This intricate field must reconcile disparate spatial and temporal scales, ranging from molecular diffusion and cellular mechanics to whole-organ hemodynamics and systemic circulation. Each level of organization introduces distinct modeling challenges, requiring tailored mathematical representations and numerical schemes [105]. The balance between accuracy, efficiency, and interpretability becomes crucial, as models must be both biologically faithful and computationally feasible. This investigation highlights key themes that have emerged in the pursuit of robust and scalable multiscale methodologies, including trade-offs between model fidelity and computational cost, challenges in numerical stability and coupling, opportunities in data-driven acceleration, and the indispensable role of verification and validation. [106]

At the smallest scales, particle-based methods such as dissipative particle dynamics (DPD), smoothed particle hydrodynamics (SPH), and molecular dynamics (MD) provide high-fidelity representations of fluid-structure interactions at the subcellular level [107]. These approaches are particularly adept at capturing complex microscale rheological phenomena, such as red blood cell (RBC) deformation, membrane fluctuations, and macromolecular transport. However, their applicability is constrained by high computational costs, limiting their ability to extend to larger biological domains [108]. In contrast, continuum-based models—such as the Navier-Stokes equations for macroscopic flow or homogenized constitutive laws for blood rheology—offer tractable representations at larger scales but risk neglecting critical microscale heterogeneities. The challenge lies in bridging these descriptions through multiscale coupling strategies, such as domain decomposition, heterogeneous multiscale methods (HMM), or hybrid particle-continuum schemes [109]. Ensuring numerical stability and consistency across these couplings is a nontrivial task, requiring specialized interface conditions and coupling operators. [110]

A fundamental limitation in high-fidelity modeling is the computational cost associated with fully resolving all scales concurrently. Adaptive meshing, multigrid techniques, and reduced-order modeling (ROM) approaches provide avenues to mitigate this burden [111]. For example, adaptive finite element methods (AFEM) can dynamically refine regions of interest, such as boundary layers near vessel walls, while coarsening elsewhere to reduce the overall computational expense. Similarly, ROM techniques, such as proper orthogonal decomposition (POD) or dynamic mode decomposition (DMD), extract dominant flow features from high-fidelity simulations, enabling reduced-order representations that retain key physical characteristics [112]. While these approaches enhance efficiency, they must be carefully designed to avoid introducing spurious numerical artifacts or losing essential biomechanical details.

The coupling of different physical processes introduces additional numerical challenges [113]. Blood flow, for instance, involves tightly coupled fluid-structure interactions (FSI) with viscoelastic vessel walls, nonlinear rheology, and biochemical transport [114]. Ensuring numerical stability in such multiphysics systems requires robust discretization strategies, such as the streamline-upwind/Petrov-Galerkin (SUPG) method for advection-dominated transport, log-conformation reformulations for viscoelastic flows, and partitioned or monolithic solvers for FSI problems. Ill-conditioned system matrices arising from these couplings necessitate efficient preconditioning strategies, such as algebraic multigrid (AMG) solvers, block-factorization techniques, or physics-informed preconditioners that exploit the underlying mathematical structure of the system. [115]

Recent advances in machine learning have introduced a

promising avenue for accelerating multiscale biofluid modeling. Data-driven surrogate models, including neural network-based approximators and Gaussian process regression, provide an alternative to direct numerical simulation in scenarios where computational costs are prohibitive [116]. These approaches have been particularly effective in capturing subgrid-scale features, such as microvascular flow patterns or tissue permeability variations, that would otherwise require prohibitively fine resolution in traditional models [117]. However, integrating these techniques into a rigorous computational framework necessitates careful training, validation, and uncertainty quantification. Machine learning models must be benchmarked against experimental data and high-fidelity simulations to ensure their predictive reliability across physiological conditions. [118]

Verification and validation remain central pillars in establishing the credibility of multiscale biofluid models. Direct comparisons with experimental measurements—ranging from in vitro microrheological assays to in vivo imaging modalities such as magnetic resonance velocimetry (MRV) and Doppler ultrasound—are essential to assess model fidelity [119]. Physiological complexity demands that these comparisons extend beyond numerical accuracy to include biologically relevant metrics, such as shear stress distributions in arteries or oxygen transport efficiency in capillary networks. Furthermore, uncertainty quantification frameworks can help delineate how parameter variability—whether stemming from patient-specific vascular geometries or cellular-scale mechanical properties—propagates through the model, affecting macroscopic flow predictions. [120]

The future of multiscale biofluid modeling lies at the intersection of computational advancements and biological integration [121]. High-performance computing (HPC) resources, including massively parallel architectures, graphics processing units (GPUs), and specialized co-processors, will continue to push the frontiers of large-scale simulation. Concurrently, advances in experimental biology, particularly single-cell omics and microfluidic assays, offer unprecedented insight into the microscale determinants of blood flow and tissue perfusion [122]. The integration of such data into continuum models holds promise for patient-specific or even genotype-specific predictive tools, enabling more precise modeling of pathological conditions such as aneurysm progression, thrombus formation, or microcirculatory dysfunction.

In the clinical and biomedical engineering domains, multiscale biofluid models are poised to play a transformative role in medical decision support and device optimization [123]. For instance, patient-specific computational fluid dynamics (CFD) simulations are increasingly used to assess surgical interventions, such as stent placements or vascular graft designs, providing quantitative predictions of hemodynamic outcomes [124]. Similarly, biofluid models inform the design of medical devices, including artificial heart valves and ventricular assist devices, ensuring optimal performance under physiologically relevant conditions. Beyond clinical applications, these models contribute to fundamental biological discovery, shedding light on emergent phenomena such as blood clot formation, immune cell transport, and mechanotransduction signaling pathways. [125]

Ultimately, the field of multiscale biofluid modeling exemplifies the intricate interplay between physics, computation, and biology. The ongoing convergence of high-fidelity simulation techniques, data-driven modeling, and high-performance computing will continue to refine our understanding of physiological flows, paving the way for new insights and applications [126]. As these methodologies mature, their transition from proof-of-concept research to clinical and biomedical impact will depend on continued efforts in model refinement, rigorous validation, and cross-disciplinary collaboration. This evolution will not only enhance our ability to simulate complex biological systems but also translate into tangible benefits in medicine, biotechnology, and healthcare innovation. [127]

References

[1] L. M. Keane, C. L. Hall, and I. R. Moyles, "An improved approximation for hydraulic conductivity for pipes of triangular cross-section by asymptotic means," *Journal of Engineering Mathematics*, vol. 126, pp. 12–, January 2021.

[2] G. Busco, R. Yang, J. Seo, and Y. A. Hassan, "10.1063/5.0019090.3," July 2020.

[3] W. Chen, L. Wang, L. Chen, H. Ge, and X. Cui, "Numerical study of the impact of glottis properties on the airflow field in the human trachea using v-les," *Respiratory physiology & neurobiology*, vol. 295, pp. 103784–, September 2021.

[4] J. Q. Feng, "Aerosol deposition in 90° circular tube bends with laminar flows: Effects of inertial impaction and gravitational settling," *Aerosol*

Science and Engineering, vol. 7, pp. 107–117, November 2022.

[5] M. A. Shabara, S. Zou, and O. Abdelkhalik, "Numerical investigation of a variable-shape buoy wave energy converter," in *Volume 9: Ocean Renewable Energy*, American Society of Mechanical Engineers, June 2021.

[6] M. Jafari, F. Hou, and A. Abdelkefi, "Wind-induced vibration of structural cables," *Nonlinear Dynamics*, vol. 100, pp. 351–421, March 2020.

[7] M. Zheng, Z. Qiuyue, Z. Zhang, L. Zhou, and T. an Zhang, *Numerical Simulation of the Influence of Particle Physical Properties on Flow Field During the Aeration Leaching Process*, pp. 43–52. Springer International Publishing, February 2021.

[8] F. Biagioli, A. Innocenti, S. Terhaar, and T. Marchione, "Experimental and numerical analysis of gas premix turbulent flames stabilized in a swirl burner with central bluff body," *Volume 4A: Combustion, Fuels, and Emissions*, vol. 143, September 2020.

[9] M. Amer, A. Vaca, and M. Bowden, "Evaluating shear in perfusion rotary lobe pump using nanoparticle aggregates and computational fluid dynamics.," *Bioprocess and biosystems engineering*, vol. 45, pp. 1477–1488, July 2022.

[10] G. Xue, X. Cheng, and A. Oztekin, "Computational study of viscoelastic flows in microchannels," in *Volume 3: Fluid Mechanics; Micro and Nano Fluid Dynamics; Multiphase Flow*, American Society of Mechanical Engineers, August 2021.

[11] R. Somassoundirame and E. Nithiyananthan, "An evolutionary optimization approach to prevent electronics burnout in subsea oil and gas equipment," *Journal of Petroleum Exploration and Production Technology*, vol. 12, pp. 1609–1623, December 2021.

[12] G. Annio, R. Torii, A. Ducci, V. Muthurangu, V. Tsang, and G. Burriesci, "Experimental validation of enhanced magnetic resonance imaging (emri) using particle image velocimetry (piv).," *Annals of biomedical engineering*, vol. 49, pp. 1–13, June 2021.

[13] B. H. Kim, K. Li, J.-T. Kim, Y. Park, H. Jang, X. Wang, Z. Xie, S. M. Won, H.-J. Yoon, G. Lee, W. J. Jang, K. H. Lee, T. S. Chung, Y. H. Jung, S. Y. Heo, Y. Lee, J. Kim, C. Tengfei, Y. Kim, P. Prasopsukh, Y. Yu, X. Yu, R. Avila, H. Luan, H. Song, F. Zhu, Y. Zhao, L. Chen, S. H. Han, J. Kim, S. J. Oh, H. Lee, C. H. Lee, Y. Huang, L. P. Chamorro, Y. Zhang, and J. A. Rogers, "Three-dimensional electronic microfliers inspired by wind-dispersed seeds.," *Nature*, vol. 597, pp. 503–510, September 2021.

[14] Z. Siddiqi and J. W. Lee, "Experimental and numerical study of novel coanda-based unmanned aerial vehicle," *Journal of Engineering and Applied Science*, vol. 69, August 2022.

[15] S. Peng, Q. Chen, and E. Liu, "The role of computational fluid dynamics tools on investigation of pathogen transmission: Prevention and control.," *The Science of the total environment*, vol. 746, pp. 142090–142090, August 2020.

[16] D. Andruczyk, R. Maingi, C. Kessel, D. Curreli, E. Kolemen, J. Canik, B. A. Pint, D. L. Youchison, and S. Smolentsev, "A domestic program for liquid metal pfc research in fusion," *Journal of Fusion Energy*, vol. 39, pp. 441–447, October 2020.

[17] A. Saraei and S. Moujaes, "The effects of exhaust air vent location on thermal comfort inside a residential building equipped with an evaporative cooling system," *Building Simulation*, vol. 14, pp. 1063–1075, December 2020.

[18] H. Aziz, S. Sansare, T. Duran, Y. Gao, and B. Chaudhuri, "On the applicability of the coarse grained coupled cfd-dem model to predict the heat transfer during the fluidized bed drying of pharmaceutical granules.," *Pharmaceutical research*, vol. 39, pp. 1991–2003, August 2022.

[19] A. Deyranlou, C. A. Miller, A. Revell, and A. Keshmiri, "Effects of ageing on aortic circulation during atrial fibrillation; a numerical study on different aortic morphologies.," *Annals of biomedical engineering*, vol. 49, pp. 1–18, March 2021.

[20] G. Nikita, B. Nishant, M. K. Gulam, and D. Vivek, "Global trends of computational fluid dynamics to resolve real world problems in the contemporary era," *Current Biochemical Engineering*, vol. 6, pp. 136–155, December 2020.

[21] D. Agarwal and G. Biros, "3d vesicle microcirculation," in *APS Division of Fluid Dynamics Meeting Abstracts*, pp. M03–034, 2019.

[22] D. C. de Oliveira, N. Abdullah, N. C. Green, and D. M. Espino, "Biomechanical assessment of bicuspid aortic valve phenotypes: A fluid–structure interaction modelling approach," *Cardiovascular engineering and technology*, vol. 11, pp. 431–447, June 2020.

[23] N. Kovacev, S. Li, S. Zeraati-Rezaei, H. Hemida, A. Tsolakis, and K. Essa, "Effects of the internal structures of monolith ceramic substrates on thermal and hydraulic properties: additive manufacturing, numerical modelling and experimental testing," *The International Journal of Advanced Manufacturing Technology*, vol. 112, pp. 1115–1132, December 2020.

[24] X. Yang, H. Wang, C. Su, X. Wang, and Y. Wang, "Heat transfer between occupied and unoccupied zone in large space building with floor-level side wall air-supply system," *Building Simulation*, vol. 13, pp. 1221–1233, May 2020.

[25] D. Reese, R. J. Thompson, R. Burns, and P. M. Danehy, "Application of femtosecond-laser tagging for unseeded velocimetry in a large-scale transonic cryogenic wind tunnel," *Experiments in Fluids*, vol. 62, pp. 1–19, April 2021.

[26] Z. Gao, W. Liang, S. Shi, and J. Zhang, "Combined heat, air, moisture and pollutant simulations (champs) research for building and urban energy efficiency and environmental quality analysis.," *Building simulation*, vol. 14, pp. 237–239, January 2021.

[27] T. G. Lim, J. H. Jung, W. H. Jeon, W. G. Joo, and G. Minorikawa, "Investigation study on the flow-induced noise by winglet and shroud shape of an axial flow fan at an outdoor unit of air conditioner," *Journal of Mechanical Science and Technology*, vol. 34, pp. 2845–2853, July 2020.

[28] X. Cui, H. Ge, W. Wu, Y. Feng, and J. Wang, "Les study of the respiratory airflow field in a whole-lung airway model considering steady respiration," *Journal of the Brazilian Society of Mechanical Sciences and Engineering*, vol. 43, pp. 1–17, February 2021.

[29] Z. Ge, W. Nemec, A. J. Vellinga, and R. L. Gawthorpe, "How is a turbidite actually deposited?," *Science advances*, vol. 8, pp. eabl9124–, January 2022.

[30] J. Qu, C. Dou, B. Xu, J. Li, Z. Rao, and A. Tsin, "Printing quality improvement for laser-induced forward transfer bioprinting: Numerical modeling and experimental validation," *Physics of Fluids*, vol. 33, pp. 071906–, July 2021.

[31] L. Zhou, C. Han, L. Bai, W. Shi, and R. K. Agarwal, "Numerical and experimental study of multiphase transient core-annular flow patterns in a spouted bed," *Journal of Energy Resources Technology*, vol. 142, June 2020.

[32] C. K. Lemmertz, R. P. Helfenstein, M. Beshir, D. Rush, W. J. V. Arnswaldt, and F. R. Centeno, "Semi-empirical correlations for predicting hot gas layer temperature in pre-flashover compartment fires considering fire source location," *Journal of the Brazilian Society of Mechanical Sciences and Engineering*, vol. 44, April 2022.

[33] G. Busco, R. Yang, J. Seo, and Y. A. Hassan, "10.1063/5.0019090.1," July 2020.

[34] H. Arastoopour, D. Gidaspow, and R. W. Lyczkowski, *Polymerization Process Intensification Using Circulating Fluidized Bed and Rotating Fluidized Bed Systems*, pp. 97–127. Springer International Publishing, August 2021.

[35] S. Pasta, C. Catalano, S. Cannata, J. M. Guccione, and C. Gandolfo, "Numerical simulation of transcatheter mitral valve replacement: The dynamic implication of lvot obstruction in the valve-in-ring case.," *Journal of biomechanics*, vol. 144, pp. 111337–111337, October 2022.

[36] D. Agarwal and G. Biros, "Stable shapes of three-dimensional vesicles in unconfined and confined poiseuille flow," *Physical Review Fluids*, vol. 5, no. 1, p. 013603, 2020.

[37] G. Fu, C. Lehrenfeld, A. Linke, and T. Streckenbach, "Locking-free and gradient-robust $h(\operatorname{div})$ -conforming hdg methods for linear elasticity," *Journal of Scientific Computing*, vol. 86, pp. 1–30, February 2021.

[38] M. J. M. M. Hoeijmakers, I. Waechter-Stehle, J. Weese, and F. van de Vosse, "Combining statistical shape modeling, cfd, and meta-modeling to approximate the patient-specific pressure-drop across the aortic

valve in real-time.," *International journal for numerical methods in biomedical engineering*, vol. 36, pp. e3387–, September 2020.

[39] S. Cuomo, V. S. D. Cola, F. Giampaolo, G. Rozza, M. Raissi, and F. Piccialli, "Scientific machine learning through physics–informed neural networks: Where we are and what's next," *Journal of Scientific Computing*, vol. 92, July 2022.

[40] M. A. Bartolo, M. U. Qureshi, M. J. Colebank, N. C. Chesler, and M. S. Olufsen, "Numerical predictions of shear stress and cyclic stretch in pulmonary hypertension due to left heart failure.," *Biomechanics and modeling in mechanobiology*, vol. 21, pp. 363–381, January 2022.

[41] Z. Li, J. Xiang, X. Liu, X. Li, L. Li, B. Shan, and R. Chen, "A combined multiscale modeling and experimental study on surface modification of high-volume micro-nanoparticles with atomic accuracy," *International Journal of Extreme Manufacturing*, vol. 4, pp. 25101–025101, February 2022.

[42] N. Pepper, A. Gaymann, S. Sharma, and F. Montomoli, "Local bi-fidelity field approximation with knowledge based neural networks for computational fluid dynamics," *Scientific reports*, vol. 11, pp. 14459–, July 2021.

[43] C.-I. Nita, A. Puiu, D. Bunescu, L. M. Itu, V. Mihalef, G. Chintalapani, A. K. Armstrong, J. D. Zampi, L. N. Benson, P. Sharma, and S. Rapaka, "Personalized pre- and post-operative hemodynamic assessment of aortic coarctation from 3d rotational angiography," *Cardiovascular engineering and technology*, vol. 13, pp. 1–27, June 2021.

[44] A. Menzer, Y. Gong, F. E. Fish, and H. Dong, "Bio-inspired propulsion: Towards understanding the role of pectoral fin kinematics in manta-like swimming.," *Biomimetics (Basel, Switzerland)*, vol. 7, pp. 45–45, April 2022.

[45] B. A. Cruden, C. Y. Tang, J. Olejniczak, A. J. Amar, and H. Tanno, "Characterization of radiative heating anomaly in high enthalpy shock tunnels," *Experiments in Fluids*, vol. 62, pp. 1–17, June 2021.

[46] D. Agarwal, M. OŃeil, and M. Rachh, "Fast multipole accelerated solvers for the laplace-beltrami problem in three dimensions," *arXiv preprint arXiv*, vol. 2111, 2021.

[47] M. O. Khan, T. Nishi, S. Imura, J. Seo, H. Wang, Y. Honda, K. Nieman, I. S. Rogers, J. A. Tremmel, J. Boyd, I. Schnittger, and A. Marsden, "Colocalization of coronary plaque with wall shear stress in myocardial bridge patients.," *Cardiovascular engineering and technology*, vol. 13, pp. 797–807, March 2022.

[48] K. Takizawa, Y. Bazilevs, and T. E. Tezduyar, "Isogeometric discretization methods in computational fluid mechanics," *Mathematical Models and Methods in Applied Sciences*, vol. 32, pp. 2359–2370, December 2022.

[49] J. A. Rodriguez-Manfredi, M. de la Torre Juarez, A. Alonso, V. Apestigue, I. Arruego, T. Atienza, D. Banfield, J. Boland, M. A. Carrera, L. Castañer, J. Ceballos, H. Chen-Chen, A. Cobos, P. G. Conrad, E. Cordoba, T. del Río-Gaztelurrutia, A. D. Vicente-Retortillo, M. Dominguez-Pumar, S. Espejo, A. G. Fairén, A. Fernández-Palma, R. Ferrandiz, F. Ferri, E. Fischer, A. García-Manchado, M. García-Villadangos, M. Genzer, S. Gimenez, J. Gómez-Elvira, F. Gómez, S. D. Guzewich, A.-M. Harri, C. Hernandez, M. Hieta, R. Hueso, I. Jaakonaho, J. J. Jiménez, V. Jiménez, A. Larman, R. Leiter, A. Lepinette, M. T. Lemmon, G. López, S. N. Madsen, T. Mäkinen, M. Marin, J. Martín-Soler, G. Martinez, A. Molina, L. Mora-Sotomayor, J. F. Moreno-Álvarez, S. Navarro, C. E. Newman, C. Ortega, M. C. Parrondo, V. Peinado, A. Peña, I. Pérez-Grande, S. Pérez-Hoyos, J. Pla-Garcia, J. Polkko, M. Postigo, O. Prieto-Ballesteros, S. C. R. Rafkin, M. Ramos, M. I. Richardson, J. Romeral, C. Romero, K. Runyon, A. Saiz-Lopez, A. Sánchez-Lavega, I. Sard, J. T. Schofield, E. Sebastián, M. D. Smith, R. Sullivan, L. K. Tamppari, A. D. Thompson, D. Toledo, F. Torrero, J. Torres, R. Urquí, T. Velasco, D. Viúdez-Moreiras, S. Zurita, and M. team, "The mars environmental dynamics analyzer, meda. a suite of environmental sensors for the mars 2020 mission," *Space science reviews*, vol. 217, pp. 48–, April 2021.

[50] S. Kim, H. Kim, W. Kim, Y. T. Cho, and N. X. Fang, "Additive manufacturing of functional microarchitected reactors for energy, environmental, and biological applications," *International Journal of Precision Engineering*

and Manufacturing-Green Technology, vol. 8, pp. 303–326, October 2020.

[51] K. M. Nagaraja, W. Li, D. Qian, V. Vasudevan, Y. Pyun, and H. Lu, "Multiphysics modeling of in situ integration of directed energy deposition with ultrasonic nanocrystal surface modification," *The International Journal of Advanced Manufacturing Technology*, vol. 120, pp. 5299–5310, March 2022.

[52] Y.-H. Loke, F. Capuano, E. Balaras, and L. J. Olivieri, "Computational modeling of right ventricular motion and intracardiac flow in repaired tetralogy of fallot," *Cardiovascular engineering and technology*, vol. 13, pp. 1–14, June 2021.

[53] J. Wedel, P. Steinmann, M. Štrakl, M. Hriberšek, and J. Ravnik, "Risk assessment of infection by airborne droplets and aerosols at different levels of cardiovascular activity.," *Archives of computational methods in engineering : state of the art reviews*, vol. 28, pp. 1–20, July 2021.

[54] A. T. Mackay and T. N. Phillips, "Compressible and nonisothermal viscoelastic flow between eccentrically rotating cylinders," *Theoretical and Computational Fluid Dynamics*, vol. 35, pp. 731–756, September 2021.

[55] S. Barwey, S. Prakash, M. Hassanaly, and V. Raman, "Data-driven classification and modeling of combustion regimes in detonation waves," *Flow, Turbulence and Combustion*, vol. 106, pp. 1065–1089, June 2020.

[56] M. Vakili and S. A. Salehi, "A review of recent developments in the application of machine learning in solar thermal collector modelling.," *Environmental science and pollution research international*, vol. 30, pp. 2406–2439, November 2022.

[57] J. R. Bhathal, F. Chassagne, L. Marsh, M. R. Levitt, C. Geindreau, and A. Aliseda, "Modeling flow in cerebral aneurysm after coils embolization treatment: A realistic patient-specific porous model approach.," *Cardiovascular engineering and technology*, vol. 14, pp. 115–128, July 2022.

[58] C. Wang and H. Luo, "A reconstructed discontinuous galerkin method for compressible flows on moving curved grids," *Advances in Aerodynamics*, vol. 3, pp. 1–28, January 2021.

[59] P. Chen, J. hao Chen, and Z. Hu, "Review of experimental-numerical methodologies and challenges for floating offshore wind turbines," *Journal of Marine Science and Application*, vol. 19, pp. 339–361, October 2020.

[60] A. Arzani, J.-X. Wang, M. S. Sacks, and S. C. Shadden, "Machine learning for cardiovascular biomechanics modeling: Challenges and beyond.," *Annals of biomedical engineering*, vol. 50, pp. 615–627, April 2022.

[61] M. das Neves Gomes, H. Salvador, F. H. Magno, A. A. Rodrigues, E. D. Santos, L. A. Isoldi, and L. A. O. Rocha, "Constructal design applied to geometric shapes analysis of wave energy converters," *Defect and Diffusion Forum*, vol. 407, pp. 147–160, March 2021.

[62] D. Agarwal, *Numerical Methods for Fast Simulation of a Red Blood Cell*. The University of Texas at Austin, 2022.

[63] P. Fillingham, M. Levitt, M. Kurt, D. Lim, E. Federico, J. Keen, and A. Aliseda, "E-177machine learning model for the prediction of patient-specific waveforms of blood flowthrough the internal carotid artery," in *SNIS 19th annual meeting electronic poster abstracts*, pp. A173.1–A173, BMJ Publishing Group Ltd., July 2022.

[64] R. Pewowaruk, J. L. Racine, J. I. Iruretagoyena, and A. Roldán-Alzate, "Ultrasound based computational fluid dynamics assessment of brachial artery wall shear stress in preeclamptic pregnancy.," *Cardiovascular engineering and technology*, vol. 11, pp. 760–768, October 2020.

[65] A. Belhocine and O. I. Abdullah, "Thermomechanical model for the analysis of disc brake using the finite element method in frictional contact," *Multiscale Science and Engineering*, vol. 2, pp. 27–41, March 2020.

[66] M. Marian, A. Almqvist, A. Rosenkranz, and M. Fillon, "Numerical micro-texture optimization for lubricated contacts—a critical discussion," *Friction*, vol. 10, pp. 1772–1809, April 2022.

[67] R. Na and Z. Shen, "Assessing cooling energy reduction potentials by retrofitting traditional cavity walls into passively ventilated cavity walls," *Building Simulation*, vol. 14, pp. 1295–1309, December 2020.

[68] Y. Wu, M. Li, J. Wang, Y. Wang, X. An, H. Fu, H. Zhang, X. Yang, and Q. Zou, "Powder-bed-fusion additive manufacturing of molybdenum: Process simulation, optimization, and property prediction," *SSRN Electronic Journal*, January 2022.

[69] C. Katinas, T. Throop, Y. C. Shin, and A. Frank, "Laser cladding of stellite-6 with a coaxial nozzle via modeling and systematic experimental investigations," *The International Journal of Advanced Manufacturing Technology*, vol. 113, pp. 837–853, January 2021.

[70] L. Bertolotti, R. Jefferson-Loveday, S. Ambrose, and E. Korsukova, "A comparison of vof and euler-euler approaches in cfd modelling of two-phase flows with a sharp interface," *Volume 2C: Turbomachinery*, pp. 1–30, September 2020.

[71] S. M. Fazeli, V. Kanjirakkad, and C. Long, "Experimental and computational investigation of flow structure in buoyancy-dominated rotating cavities," *Journal of Engineering for Gas Turbines and Power*, vol. 143, March 2021.

[72] A. R. Esmaeili, B. Sajadi, and M. Akbarzadeh, "Numerical simulation of ellipsoidal particles deposition in the human nasal cavity under cyclic inspiratory flow," *Journal of the Brazilian Society of Mechanical Sciences and Engineering*, vol. 42, pp. 1–13, April 2020.

[73] T. Muther, A. K. Dahaghi, F. I. Syed, and V. V. Pham, "Physical laws meet machine intelligence: current developments and future directions," *Artificial Intelligence Review*, vol. 56, pp. 6947–7013, December 2022.

[74] V. Ramesh, S. Terala, S. Mazumder, G. Matharu, V. D. P, and S. K. Ali, "Development and validation of a model for efficient simulation of freezing of water in large tanks," *Journal of Thermal Science and Engineering Applications*, vol. 13, June 2020.

[75] A. Kazemi, D. A. Padgett, S. Callahan, M. Stoddard, and A. A. Amini, "Relative pressure estimation from 4d flow mri using generalized bernoulli equation in a phantom model of arterial stenosis.," *Magma (New York, N.Y.)*, vol. 35, pp. 733–748, February 2022.

[76] D. Agarwal and G. Biros, "Shape dynamics of a red blood cell in poiseuille flow," *Physical Review Fluids*, vol. 7, no. 9, p. 093602, 2022.

[77] A. Bamido, V. K. Dhir, V. Prasad, and D. Banerjee, "A numerical study of forced convective heat transfer characteristics of supercritical fluid in a horizontal circular-pipe," in *ASME 2020 Heat Transfer Summer Conference*, American Society of Mechanical Engineers, July 2020.

[78] T. Davydzenka and P. Tahmasebi, "High-resolution fluid–particle interactions: a machine learning approach," *Journal of Fluid Mechanics*, vol. 938, March 2022.

[79] M. B. Okuducu and M. M. Aral, "Toward the next generation of passive micromixers: A novel 3-d design approach.," *Micromachines*, vol. 12, pp. 372–, March 2021.

[80] D. Niedermeier, J. Voigtländer, S. Schmalfuß, D. Busch, J. Schumacher, R. A. Shaw, and F. Stratmann, "Characterization and first results from lacis-t: a moist-air wind tunnel to study aerosol–cloud–turbulence interactions," *Atmospheric Measurement Techniques*, vol. 13, pp. 2015–2033, April 2020.

[81] S. Chandrasekaran, M. Si, J. Zhai, and L. Oden, "Special issue on new trends in high-performance computing: Software systems and applications," *Software: Practice and Experience*, vol. 53, pp. 3–5, October 2022.

[82] J. van Batenburg-Sherwood and S. Balabani, "Continuum microhaemodynamics modelling using inverse rheology.," *Biomechanics and modeling in mechanobiology*, vol. 21, pp. 335–361, December 2021.

[83] Y. Liu and J. J. Sansalone, "Physically-based particle size distribution models of urban water particulate matter," *Water, Air, & Soil Pollution*, vol. 231, pp. 1–19, November 2020.

[84] L. Li, M. Nagy, J. M. Graving, J. B. Bak-Coleman, G. Xie, and I. D. Couzin, "Vortex phase matching as a strategy for schooling in robots and in fish.," *Nature communications*, vol. 11, pp. 5408–5408, October 2020.

[85] A. A. Shoukat, U. M. Chaudry, M. Shaban, M. Anwar, T. I. Khan, H. W. Ahmad, and R. Mujahid, "Flow rate optimization for thermal-fsi of minichannel heat sink: A numerical approach," *Arabian Journal for Science and Engineering*, vol. 46, pp. 7577–7586, March 2021.

[86] M. U. Ghori, J. S. Nirwan, T. Asim, Y. Chahid, S. Farhaj, Z. Khizer, P. Timmins, and B. R. Conway, "Muco-dis: a new afm-based nanoscale dissolution technique," *AAPS PharmSciTech*, vol. 21, pp. 142–, May 2020.

[87] V. Sobes, B. Hiscox, E. L. Popov, R. Archibald, C. D. Hauck, B. R. Betzler, and K. A. Terrani, "Ai-based design of a nuclear reactor core," *Scientific reports*, vol. 11, pp. 1–9, October 2021.

[88] J. Bagge, G. Biros, and D. Agarwal, "Gpu-accelerated simulation of deformable capsules flowing through a pipe," 2024.

[89] D.-H. Kim, Y. Sanada, H. Sadat-Hosseini, and F. Stern, "Urans simulations for a free-running container ship: Part 2. added power," *Journal of Hydrodynamics*, vol. 33, pp. 448–467, July 2021.

[90] F. Jia, Z. Y. Li, D. Y. Pui, and C. J. Tsai, "A detailed numerical study on the evolution of droplet size distribution of dibutyl phthalate in a laminar flow diffusion chamber," *Korean Journal of Chemical Engineering*, vol. 37, pp. 423–433, March 2020.

[91] T. May, B. Eslami, and K. Fouladi, "Optimization of 3d printer enclosure environment," *The International Journal of Advanced Manufacturing Technology*, vol. 118, pp. 2233–2246, September 2021.

[92] J. Finnigan, K. W. Ayotte, I. N. Harman, G. G. Katul, H. J. Oldroyd, E. G. Patton, D. Poggi, A. N. Ross, and P. A. Taylor, "Boundary-layer flow over complex topography," *Boundary-Layer Meteorology*, vol. 177, pp. 247–313, October 2020.

[93] M. Foukrach, M. Bouzit, H. Ameur, and Y. Kamla, "Effect of agitator's types on the hydrodynamic flow in an agitated tank," *Chinese Journal of Mechanical Engineering*, vol. 33, pp. 1–18, May 2020.

[94] L. Yang, T. Neuberger, and K. B. Manning, "In vitro real-time magnetic resonance imaging for quantification of thrombosis," *Magma (New York, N.Y.)*, vol. 34, pp. 285–295, July 2020.

[95] N. C. Lima, W. R. Assis, C. A. Alvarez, and E. de Moraes Franklin, "10.1063/5.0121810.1," December 2022.

[96] Z. Zhao, L. Zhao, and S.-Y. Lee, "Evaluation of soot production near a cold surface for an impinged diesel spray combustion," in *ASME 2020 Internal Combustion Engine Division Fall Technical Conference*, American Society of Mechanical Engineers, November 2020.

[97] H. Hatoum, S. Singh-Gryzbon, F. Esmailie, P. Ruile, F.-J. Neumann, P. Blanke, V. H. Thourani, A. P. Yoganathan, and L. P. Dasi, "Predictive model for thrombus formation after transcatheter valve replacement.," *Cardiovascular engineering and technology*, vol. 12, pp. 576–588, December 2021.

[98] G. Vigne, W. Wegrzyński, A. Cantizano, P. Ayala, G. Rein, and C. Gutiérrez-Montes, "Experimental and computational study of smoke dynamics from multiple fire sources inside a large-volume building," *Building Simulation*, vol. 14, pp. 1147–1161, September 2020.

[99] G. Kumaran, R. Sivaraj, V. R. Prasad, O. A. Bég, H.-H. Leung, and F. Kamalov, "Numerical study of axisymmetric magneto-gyrotactic bioconvection in non-fourier tangent hyperbolic nano-functional reactive coating flow of a cylindrical body in porous media," *The European Physical Journal Plus*, vol. 136, pp. 1107–, November 2021.

[100] L. Zhang, S. R. Ray, and M. Zangeneh, "Application of 3d inverse design method on a transonic compressor stage," in *Volume 10C: Turbomachinery — Design Methods and CFD Modeling for Turbomachinery; Ducts, Noise, and Component Interactions*, American Society of Mechanical Engineers, June 2022.

[101] K. Javanroodi, V. M. Nik, M. G. Giometto, and J.-L. Scartezzini, "Combining computational fluid dynamics and neural networks to characterize microclimate extremes: Learning the complex interactions between meso-climate and urban morphology.," *The Science of the total environment*, vol. 829, pp. 154223–154223, March 2022.

[102] D. S. de Araujo, D. H. M. de Moraes, M. Mesquita, R. A. Flores, R. Battisti, G. G. Santos, F. P. de Deus, and R. S. Ferrarezi, "Numerical modeling of microfluid dynamics in xylem vessels of khaya grandifoliola," *Water*, vol. 13, pp. 2723–, October 2021.

[103] D. Agarwal and G. Biros, "Numerical simulation of an extensible capsule using regularized stokes kernels and overset finite differences," *Journal of Computational Physics*, vol. 509, p. 113042, 2024.

[104] J. Fang, D. Shaver, and E. Merzari, "Modeling the effect of spacer grid and mixing vanes in coupled cfd simulations of small modular reactors," in *Volume 3: Computational Fluid Dynamics; Micro and Nano Fluid Dynamics*, American Society of Mechanical Engineers, July 2020.

[105] B. E. Abali and O. Savas, "Experimental validation of computational fluid dynamics for solving isothermal and incompressible viscous fluid flow," *SN Applied Sciences*, vol. 2, pp. 1–16, August 2020.

[106] E. B. Baker, J. Nawer, X. Xiao, and D. M. Matson, "Mhd surrogate model for convection in electromagnetically levitated molten metal droplets processed using the iss-eml facility.," *NPJ microgravity*, vol. 6, pp. 9–9, March 2020.

[107] I. T. Ali, I. Afgan, and I. Khurshid, "Stratified two-phase turbulent pipe flow simulations," *International Journal on Advanced Science, Engineering and Information Technology*, vol. 12, pp. 1301–1301, August 2022.

[108] J. McCraney, M. Weislogel, and P. Steen, "Capillary flow experiments conducted aboard the international space station: Experiments and simulations," *Microgravity Science and Technology*, vol. 34, July 2022.

[109] R. Prather, A. Das, M. Farias, E. Divo, A. Kassab, and W. DeCampli, "Parametric investigation of an injection-jet self-powered fontan circulation.," *Scientific reports*, vol. 12, pp. 2161–, February 2022.

[110] B. Fotovvati, S. Rauniyar, J. A. Arnold, and K. Chou, "Experimental, computational, and data-driven study of the effects of selective laser melting (slm) process parameters on single-layer surface characteristics," *The International Journal of Advanced Manufacturing Technology*, vol. 123, pp. 119–144, September 2022.

[111] J. Reyes, D. Fontes, A. Bazzi, M. Otero, K. Ahmed, and M. P. Kinzel, "Effect of saliva fluid properties on pathogen transmissibility.," *Scientific reports*, vol. 11, pp. 16051–16051, August 2021.

[112] Z. Liu and C. Copeland, "Optimization of a radial turbine for pulsating flows," *Journal of Engineering for Gas Turbines and Power*, vol. 142, April 2020.

[113] Z. A. Wei, B. Si, X. Ge, M. Zhu, M. A. Cetatoiu, C. Tian, L. Sun, and B. Qiao, "Is doppler echocardiography adequate for surgical planning of single ventricle patients," *Cardiovascular engineering and technology*, vol. 12, pp. 1–12, April 2021.

[114] A. Bouziane, A. Alami, M. Zaitri, B. Bouchame, and M. Bouchetara, "Investigation of swirl stabilized ch4 air flame with varied hydrogen content by using computational fluid dynamics (cfd) to study the temperature field and flame shape," *Engineering, Technology & Applied Science Research*, vol. 11, pp. 6943–6948, April 2021.

[115] I. Janajreh, S. Elagroudy, C. Ghenai, S. S. Raza, I. Adeyemi, and K. Moustakas, "Gasification of spent pot-lining from the aluminum industry," *SN Applied Sciences*, vol. 3, pp. 1–16, March 2021.

[116] A. R. Kumar, S. Schafrik, and O. Velasquez, "Designing, modeling, and laboratory testing of a non-clogging impingement type filter for mining dust scrubbers," *Mining, Metallurgy & Exploration*, vol. 37, pp. 1911–1918, September 2020.

[117] Z. Lu, E. D. Dupuis, V. K. Patel, A. M. Momen, and S. Shahab, "Ultrasonic oscillatory two-phase flow in microchannels," *Physics of Fluids*, vol. 33, pp. 032003–, March 2021.

[118] M. Dickison, M. Ghaleeh, S. Milady, L. T. Wen, and M. A. Qubeissi, "Investigation into the aerodynamic performance of a concept sports car," *Journal of Applied Fluid Mechanics*, vol. 13, pp. 583–601, March 2020.

[119] Y. Tang, X. Yang, W. Liu, L. Qi, Y. Wang, and Y. Wang, "Design and analysis of a novel swimming mechanism inspired from frogs," *Journal of Intelligent & Robotic Systems*, vol. 105, May 2022.

[120] C. Zhao, X. Pei, and X. Liu, "Computational investigation on void defects formation and periodic tool-workpiece sliding-to-sticking transition in self-reacting friction stir welding," *The International Journal of Advanced Manufacturing Technology*, vol. 120, pp. 8075–8088, May 2022.

[121] F. Alamshahi, H. Rahimzadeh, R. Rafee, M. Moghimi, and P. Talebizadehsardari, "Effects

of roughness on the performance of a threaded zigzag demister using rsm and k turbulent models," *Sādhanā*, vol. 45, pp. 1–14, November 2020.

[122] A. Palacio-Betancur and M. G. Soto, "Recent advances in computational methodologies for real-time hybrid simulation of engineering structures," *Archives of Computational Methods in Engineering*, vol. 30, pp. 1637–1662, November 2022.

[123] G. Busco, R. Yang, J. Seo, and Y. A. Hassan, "Sneezing and asymptomatic virus transmission," *Physics of fluids (Woodbury, N.Y. : 1994)*, vol. 32, pp. 073309–073309, July 2020.

[124] G. Yan, Z. Li, T. Bore, S. G. Torres, A. Scheuermann, and L. Li, "Discovery of dynamic two-phase flow in porous media using two-dimensional multiphase lattice boltzmann simulation," *Energies*, vol. 14, pp. 4044–, July 2021.

[125] X. Zhang, J. Gomez-Paz, X. Chen, J. M. McDonough, M. M. Islam, Y. Andreopoulos, L. Zhu, and H. Yu, "Volumetric lattice boltzmann method for wall stresses of image-based pulsatile flows.," *Scientific reports*, vol. 12, pp. 1697–, February 2022.

[126] K. C. Kalvakala, P. Pal, Y. Wu, G. Kukkadapu, C. P. Kolodziej, J. P. Gonzalez, M. U. Waqas, T. Lu, S. K. Aggarwal, and S. Som, "Numerical analysis of fuel effects on advanced compression ignition using a cooperative fuel research engine computational fluid dynamics model," *Journal of Energy Resources Technology*, vol. 143, March 2021.

[127] J. Messler, N. Husser, and S. Brizzolara, "The impacts of model uncertainty on rans cfd simulations of a high-speed craft," in *Day 1 Tue, October 26, 2021*, SNAME, October 2021.